Epithelial p53 Status Modifies Stromal-Epithelial Interactions During Basal-Like Breast Carcinogenesis

Ashley M. Fuller[1,6] · Lin Yang[2] · Alina M. Hamilton[1] · Jason R. Pirone[3,7] · Amy L. Oldenburg[2,4] ·
Melissa A. Troester[1,4,5]

Abstract

Basal-like breast cancers (BBC) exhibit subtype-specific phenotypic and transcriptional responses to stroma, but little research has addressed how stromal-epithelial interactions evolve during early BBC carcinogenesis. It is also unclear how common genetic defects, such as p53 mutations, modify these stromal-epithelial interactions. To address these knowledge gaps, we leveraged the MCF10 progression series of breast cell lines (MCF10A, MCF10AT1, and MCF10DCIS) to develop a longitudinal, tissue-contextualized model of p53-deficient, pre-malignant breast. Acinus asphericity, a morphogenetic correlate of cell invasive potential, was quantified with optical coherence tomography imaging, and gene expression microarrays were performed to identify transcriptional changes associated with p53 depletion and stromal context. Co-culture with stromal fibroblasts significantly increased the asphericity of acini derived from all three p53-deficient, but not p53-sufficient, cell lines, and was associated with the upregulation of 38 genes. When considered as a multigene score, these genes were upregulated in co-culture models of invasive BBC with increasing stromal content, as well as in basal-like relative to luminal breast cancers in two large human datasets. Taken together, stromal-epithelial interactions during early BBC carcinogenesis are dependent upon epithelial p53 status, and may play important roles in the acquisition of an invasive morphologic phenotype.

Keywords Co-culture · Fibroblast · MCF10 series · Optical coherence tomography · 3D culture

Abbreviations

ADH	Atypical ductal hyperplasia
BBC	Basal-like breast cancer
DCIS	Ductal carcinoma in situ
ER	Estrogen receptor
FDR	False discovery rate
FEA	Flat epithelial atypia
OCT	Optical coherence tomography
PR	Progesterone receptor
RMF	Reduction mammoplasty fibroblast
TCGA	The Cancer Genome Atlas
*	Protein truncation
LOH	Loss of heterozygosity

✉ Melissa A. Troester
troester@unc.edu

1   Department of Pathology and Laboratory Medicine, The University of North Carolina, Chapel Hill, NC 27599, USA

2   Department of Physics and Astronomy, The University of North Carolina, Chapel Hill, NC 27599, USA

3   School of Pharmacy, The University of North Carolina, Chapel Hill, NC 27599, USA

4   Lineberger Comprehensive Cancer Center, The University of North Carolina, Chapel Hill, NC 27599, USA

5   Department of Epidemiology, Gillings School of Global Public Health, The University of North Carolina, Chapel Hill, NC 27599, USA

6   Department of Pathology and Laboratory Medicine, Abramson Family Cancer Research Institute, Penn Sarcoma Program, The University of Pennsylvania Perelman School of Medicine, Philadelphia, PA 19104, USA

7   Nuventra Pharma Sciences, Durham, NC 27713, USA

Introduction

Breast carcinogenesis occurs in a stepwise fashion, with flat epithelial atypia (FEA), atypical ductal hyperplasia (ADH), and ductal carcinoma in situ (DCIS) recognized as *bona fide*, non-obligate precursors to invasive and/or metastatic disease [1, 2]. Risk stratification of these early lesions has been challenging, with few studies identifying robust markers for high-risk FEA or ADH. A genomic assay (Oncotype DX DCIS score) is now clinically available for

risk stratification of DCIS, and emphasizes genomic markers corresponding to cell proliferation. However, the role of the tumor microenvironment in early lesion progression is less commonly studied. Due to the paucity of tissue samples from women with early pre-invasive lesions, as well as limited follow-up data in previous cohort studies [3-7], there are many knowledge gaps pertaining to the evolution of stromal-epithelial interactions during breast carcinogenesis.

Previous research in our group has shown that pre-malignant basal-like breast cancer (BBC) cell lines exhibit unique morphologic responses in the context of stroma. Specifically, we employed three-dimensional (3D) culture models and optical coherence tomography (OCT), a quantitative imaging technique analogous to ultrasound that uses light instead of sound, to demonstrate that DCIS, but not benign, basal-like acini became more aspherical in the presence of fibroblasts [8]. Asphericity describes the extent to which acinus morphology deviates from that of a perfect sphere, and correlates with cell invasive potential [8, 9]. Basal-like cancers also have unique molecular features, including high rates of loss-of-function (nonsense and frame shift) mutations in *TP53* (p53) and other components of the p53 pathway [10-12]. However, very little is known about effects of specific BBC cell genetic defects on stromal-epithelial interactions, particularly in the setting of early pre-invasive disease.

We hypothesized that epithelial p53 status modifies stromal-epithelial interactions during BBC carcinogenesis, with effects on multicellular morphology and gene expression. We depleted *TP53* expression in the pre-malignant MCF10 progression series, an isogenic series of breast epithelial cell lines that, in xenograft models, recapitulates features of pre-invasive basal-like lesions including benign change (MCF10A), ADH (MCF10AT1), and comedogenic DCIS (MCF10DCIS.com, herein referred to as MCF10DCIS) [13-18]. Using 3D culture models, OCT imaging, and whole-genome microarrays, we evaluated acinus asphericity and gene expression to identify stroma-mediated phenotypic and transcriptional patterns associated with progression of early pre-invasive BBC.

Materials and Methods

Cell Lines

The basal-like isogenic MCF10 progression series (MCF10A, MCF10AT1, and MCF10DCIS) was obtained from the Barbara Ann Karmanos Cancer Institute (Detroit, MI). Initially generated via transfection with activated *HRAS* and subsequent serial passaging in mice, these increasingly transformed cell lines express a mutant oncogene found at low prevalence among human BBC cases, but are nevertheless useful models for studying progression to invasive disease [14, 19]. Cells were found to be negative for mycoplasma contamination at the beginning of this study. Similar to previous studies [9, 20], we also utilized an hTERT-immortalized reduction mammoplasty fibroblast (RMF) cell line (a gift from Charlotte Kuperwasser, PhD; Tufts University Medical Center, Boston, MA) to circumvent the variability and phenotypic heterogeneity of primary human fibroblasts. Additional details are provided in the Electronic Supplementary Material file.

Generation of p53-knockdown MCF10 Series Cell Lines

shRNA plasmids generated by Masutomi and colleagues [21] were purchased from Addgene (pMKO.1-puro-p53 shRNA 2 [Addgene #10672] and pMKO.1-puro-GFP shRNA [Addgene #10675]). Plasmids were transfected into Phoenix-AMPHO packaging cells (ATCC, Manassas, VA) using Lipofectamine LTX (Invitrogen) according to the manufacturers' instructions, and the virus-containing supernatants were directly applied to each of the parent MCF10 series cell lines. Stable populations were established by selection in 1 µg/mL puromycin for 14 days.

3D Culture Conditions and Microscopy

Cells were suspended in a biologically derived matrix comprised of 50% phenol red-free Matrigel (#356,237; Corning, Corning, NY) and 50% rat-tail collagen I (#354,236; Corning) diluted to a final concentration of 1 mg/mL as previously described [8, 9, 22, 23]. Suspended cells were then seeded into tissue culture plates pre-coated with the same matrix, and growth medium was dispensed to the apical side of each culture after 30–60 min. Cultures were constructed with the same total starting cell number (30,000 cells/mL for mono-cultures; 15,000 breast cells/mL + 15,000 RMFs/mL for co-cultures), rather than the same starting number of breast cells, to reduce the potential for nutrient deprivation in co-cultures. RMF mono-cultures (30,000 cells/mL) were generated as normalization controls for gene expression microarray analyses (see below). Cultures were refreshed with MCF10 growth medium every 2–3 days, and maintained for 14 days. Brightfield micrographs of 3D acini were acquired using a Nikon Eclipse TS100 microscope and Nikon NIS-Elements version 4.30 software (Melville, NY). Acircularity index [24], defined as the ratio of the perimeter of a given acinus to the circumference of a perfect circle with the same cross-sectional area of the acinus, was computed with ImageJ.

OCT-based Morphology Assay and Image Analysis

Acinus asphericity, a morphologic correlate of cell invasive potential [8, 9], was quantified using OCT imaging. Asphericity is defined as the ratio of the volume of a perfect sphere with the same surface area as a given acinus to the volume of the acinus; a value of 1 signifies a perfectly spherical structure, whereas values greater than 1 indicate morphologic divergence from a perfect sphere [8]. The imaging platform used in the present study was a spectral-domain OCT system that has been modified slightly from that described previously [8]. The system employed a Ti:Sapphire laser with a center wavelength and bandwidth of 800 nm and 120 nm, respectively, to provide ~ 6 mW of light to the sample. Spectral interferograms (200 frames per sample) were captured with a line scan CCD camera (Basler Sprint) operated at 5 kHz, providing a signal-to-noise ratio of 108 dB, and a resolution of $10.0~\mu m \times 3.0~\mu m$ (lateral [x,y] by axial [z]) in aqueous medium. Each 3D culture was sampled over a volume of $3~mm \times 1.5~mm \times 1.55~mm$ into $1000 \times 200 \times 1024$ pixels in $x \times y \times z$, and stored as a stack of 2D (x–z) image slices. Image stacks were subsequently examined in IrfanView to manually tabulate approximate (x,y,z) locations of the centers of acini. These positions were then input into a custom, semi-automated segmentation program and graphical user interface written in MATLAB to segment the shape of each acinus, as follows: First, volumetric regions of interest (ROIs) centered around each acinus were upsampled in x and y to achieve an isotropic pixel size of 1.5 μm, then mean-filtered in x and z with a window size of 15 μm. The user then selected an intensity threshold for each ROI based upon histogram analysis of pixel intensities to best segment the acinus from the surrounding matrix (background). The program subsequently filled in any holes enclosed by acinus boundaries. The segmented surface area, provided by the size of the output of "isosurface" in MATLAB, was multiplied by a factor of 2/3 to correct for pixel connectivity. Subsequently, the asphericity was computed. To avoid selection bias, acini that met all of the following criteria were analyzed: 1) did not overlap with adjacent structures; 2) were not in close proximity to the edge of an image frame or the apical surface of the culture matrix; and 3) could be adequately distinguished from background. On average, approximately 15 acini per independent experiment were analyzed for each culture condition (n = 2–5 independent experiments). Acini generated for OCT imaging were not utilized in microarray experiments (see below) to circumvent the possible transient effects of the imaging process on gene expression.

Whole Genome Microarrays and Data Analysis

RNA sample quality was determined using the Agilent Tape Station (Santa Clara, CA). All samples had RNA integrity numbers of > 7. Samples were labeled and amplified using the Agilent Low Input Two-Color, QuickAmp Labeling kit (#5190–2306). Cy-5-labeled cDNAs were generated from all experimental samples, and reference RNA (Stratagene Universal Human Reference spiked 1:1000 with MCF-7 RNA and 1:1000 with ME16C RNA to increase expression of breast cancer genes) was labeled with Cy-3. All samples were run in duplicate (2 independent experiments) on Agilent human 4×44 K v2 whole genome microarrays (#G4845A), with the exception of RMF mono-cultures: due to low sample concentrations, RNA from 4 wells from 2 independent experiments was pooled, concentrated, and applied to each of 4 microarrays. Microarray data have been deposited in the Gene Expression Omnibus under the accession number GSE162553.

Microarray data were Lowess-normalized, and probes with signal > 10 dpi in both channels and data present in at least 80% of samples were selected for further analysis. During data pre-processing, we: 1) eliminated probes without corresponding ENTREZ Gene IDs; 2) collapsed duplicate probes corresponding to the same ENTREZ Gene ID by averaging; and 3) imputed missing data using the k-nearest neighbors' imputation with $k = 10$. Unless otherwise specified, analyses of median-centered expression data were conducted with significance analysis of microarrays (SAM) procedures on the top ~ 20–30% most variable genes in each comparison; details pertaining to specific analyses are provided in the text. SAM analyses were carried out in R, version 3.5.2, and data visualization was performed using Cluster 3.0 and Java TreeView.

For co-cultures, we noted that the higher proliferation rate of breast epithelial cells relative to fibroblasts would likely alter relative cell proportions in these samples. Therefore, we utilized the method of Buess et al. [9, 20, 25] to estimate the proportion of fibroblasts in the final co-cultures. This expression deconvolution approach estimates the percentage of cancer cells and fibroblasts in each co-culture, normalizes the resulting data for additive effects in the mixed-composition co-culture sample, and calculates a coefficient of interaction ("I") for each gene by determining the ratio of observed to expected co-culture gene expression. We used this approach to generate an I-matrix consisting of interaction coefficients for each gene in all co-cultures, which can be analyzed in an identical manner to non-co-culture-normalized microarray data. This analysis revealed that RMF contributions to gene expression were extremely limited and not highly variable across experiments after two weeks in 3D culture. Therefore, given the stable levels and relative abundance of epithelium across co-cultures, further normalization of gene expression data to account for differences in relative cell proportions was not required.

Progression Gene Signature: Derivation and Sample Scoring

A 38-gene, cell-based "progression signature" was developed via a 2-class, unpaired SAM analysis comparing MCF10A-sh:p53, MCF10AT1-sh:p53, and MCF10DCIS-sh:p53 co-cultures to the corresponding mono-cultures; this gene signature represents a common transcriptional response elicited in p53-knockdown co-cultures by the presence of fibroblasts. Samples from 3 independent datasets (see below) were then scored for the progression signature using the method of Creighton et al. [26], with modifications: Briefly, since each gene in the progression signature was upregulated in co-cultures compared to mono-cultures, the $\log_2$-transformed, median-centered expression levels of all genes in the signature were averaged to generate a "progression score". Functional analysis was performed with Ingenuity Pathway Analysis (IPA; Redwood City, CA) with Benjamini–Hochberg correction for multiple comparisons. The progression signature was evaluated in The Cancer Genome Atlas (TCGA) [12] and METABRIC [27] breast cancer datasets (n = 1054 and 1689, respectively, excluding tumor samples classified as the "normal-like" subtype), as well as in a cell-based dataset of invasive breast cancer microenvironments reported by Camp and colleagues [20]. Datasets were cleaned and normalized as described above, except that probes were filtered to those with expression in > 70% of samples.

Statistics

Statistical analyses were performed with GraphPad Prism, version 8.0 (GraphPad Inc., La Jolla, CA). Details pertaining to specific tests are indicated in the text and figure legends. Error bars indicate the mean + standard error of the mean (SEM), and $P < 0.05$ was considered statistically significant.

Results

Phenotypic Characterization of p53-deficient MCF10 Series

To study effects of p53 deficiency on pre-malignant BBC cells, a p53-targeting shRNA (herein referred to as "sh:p53") was stably expressed in MCF10A, MCF10AT1, and MCF10DCIS cells. Consistent with previous literature [28-31], we confirmed that the 3 parent lines expressed wild-type *TP53* (not shown). Stable lines expressing a control, GFP-targeting shRNA ("sh:GFP") were also generated. qRT-PCR indicated that *TP53* expression was reduced by > 80% for each p53-deficient cell line (Fig. 1a). Additionally, analyses of cells grown on plastic demonstrated that cell

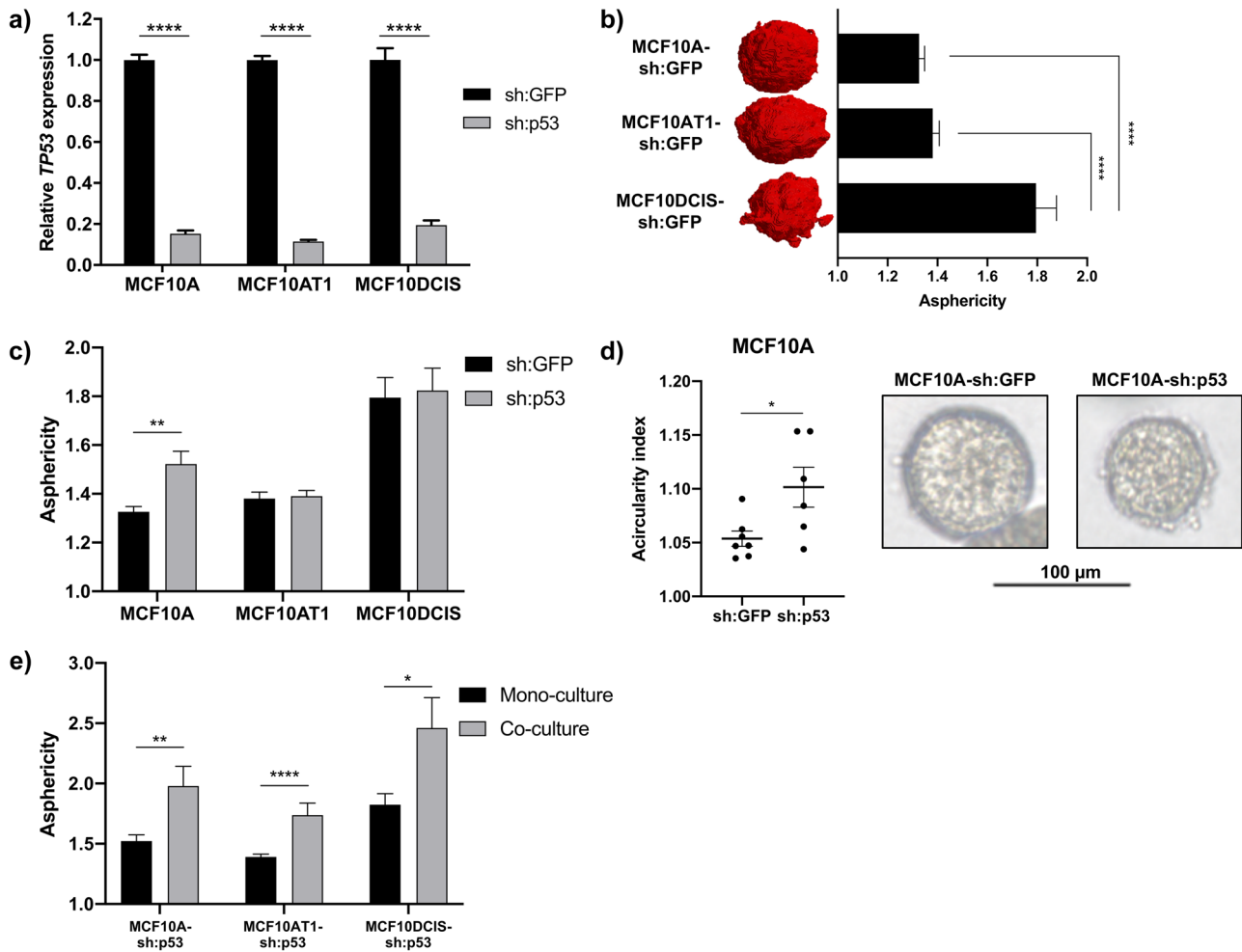proliferation did not significantly differ between members of each isogenic pair (Suppl. Figure 1).

Using our previously validated OCT imaging system [8,9], we studied asphericity as a correlate of cell invasive potential. Figure 1b demonstrates that asphericity correlated with progression, with MCF10DCIS-sh:GFP acini being significantly more aspherical than both MCF10AT1-sh:GFP and MCF10A-sh:GFP acini. MCF10AT1-sh:GFP acini also tended (but not significantly) to be more aspherical than MCF10A-sh:GFP acini. We then characterized the morphogenetic responses of pre-invasive BBC cells to *TP53* knockdown. The morphologic characteristics of MCF10AT1 and MCF10DCIS acini were not altered by p53 depletion. However, the asphericity of MCF10A acini, the most spherical cultures in the setting of p53-sufficiency, significantly increased upon *TP53* knockdown (Fig. 1c). In support of this finding, 2D photomicrographs of MCF10-sh:GFP and MCF10-sh:p53 3D culture also revealed that *TP53*-deficient acini displayed an elevated cross-sectional acircularity index relative to control acini (Fig. 1d).

Morphologic Responses of p53-deficient MCF10 Acini to Stroma

To assess acinus morphometry in the context of stromal signals, OCT-based morphogenesis analyses were performed on epithelial cell-RMF co-cultures (seeded at a 1:1 ratio). Consistent with previous results [8], among the p53-sufficient cell lines, the presence of fibroblasts significantly increased the asphericity of MCF10DCIS-sh:GFP acini (Suppl. Figure 2); neither MCF10A-sh:GFP nor MCF10AT1-sh:GFP acini showed this pattern. In contrast, morphologic responses to stroma were more pronounced among the p53-knockdown MCF10 lines, with fibroblast co-culture significantly increasing the asphericity of all three p53-deficient acini (MCF10A, MCF10AT1, and MCF10DCIS; Fig. 1e).

Transcriptional Changes Correlating with Morphologic Responses of p53-deficient Acini to Stroma

To identify transcriptional patterns associated with the observed morphologic effects, we performed gene expression microarray analyses on MCF10 acini 1) upon knockdown of *TP53* and 2) in the context of both *TP53* knockdown and stromal milieu. When we compared the gene expression profiles of p53-deficient and -sufficient acini (qPCR-based validation of *TP53* expression in these 3D cultures is shown in Suppl. Figure 3a), minimal transcriptional changes were observed in response to *TP53* knockdown: Two-class SAM analyses of the top ~ 10% most variable genes demonstrated that *TP53* knockdown did not significantly
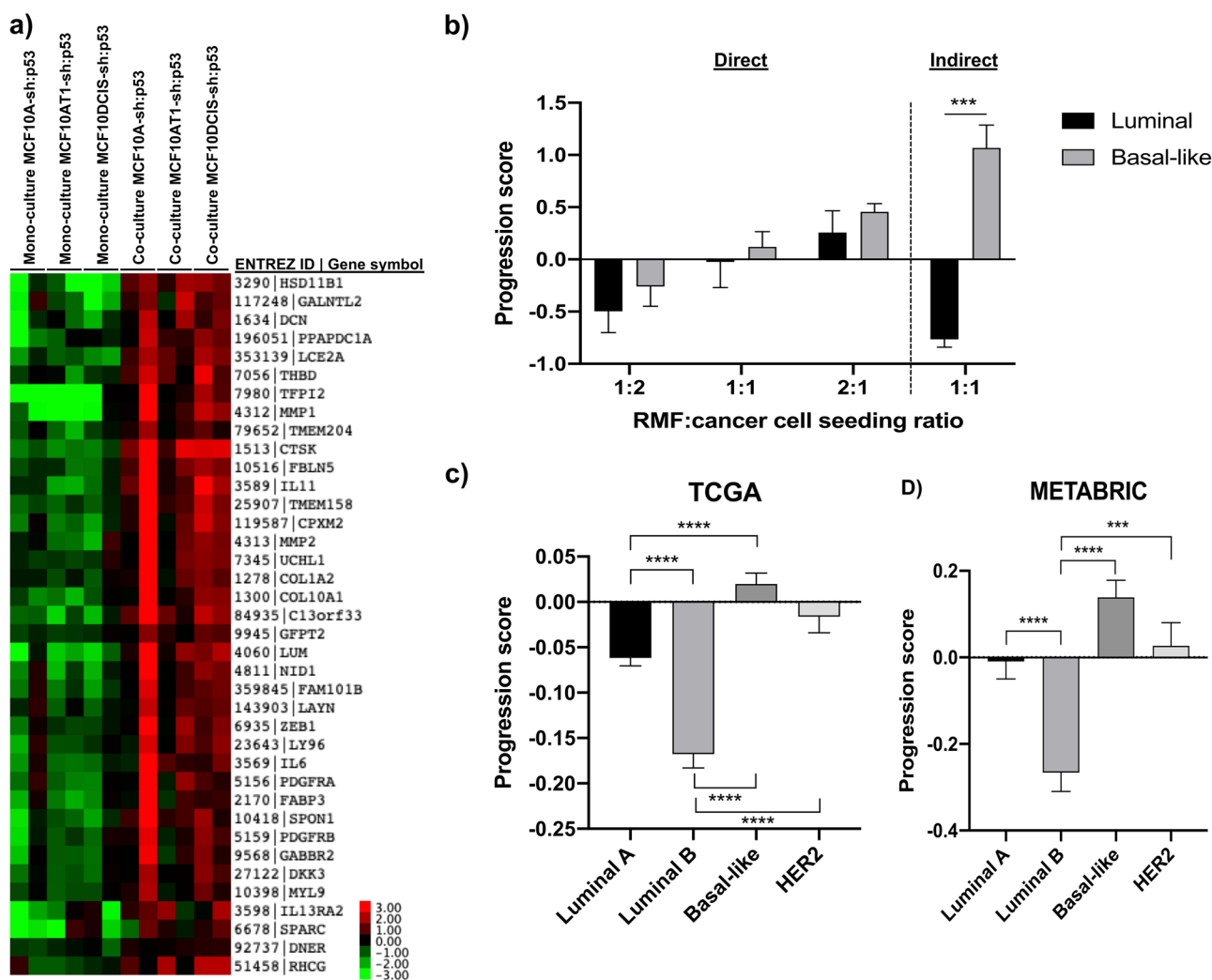
Fig. 1 Morphologic responses of MCF10 series acini to p53 deficiency and stromal context. **a**) *TP53* gene expression in MCF10 series cells stably expressing a p53-targeting shRNA (sh:p53) or GFP-targeting control shRNA (sh:GFP). ****p < 0.0001. Number of t tests: 3. n = 3 independent experiments. **b**) Asphericity and representative 3D renderings of sh:GFP MCF10 series acini. ****p < 0.0001 by one-way ANOVA with Tukey's multiple comparisons test. n = 5 independent experiments. **c**) Asphericity of MCF10 series acini in response to *TP53* knockdown. **p = 0.005805. Number of t tests: 3. n = 5 independent experiments. **d**) *Left:* Cross-sectional acicular-ity indices of MCF10A acini. *p = 0.0271 by two-tailed t-test. *Right:* Representative photomicrographs of MCF10A acini in cross-section. **e**) Asphericity of p53-deficient MCF10 series acini in the presence of fibroblasts. *p < 0.05; **p < 0.01; ****p < 0.0001. Number of t tests: 6; data were analyzed together with that in Suppl. Figure 2, but were graphed separately for visualization purposes. n = 2–5 independent experiments. For panels a, c, and e, statistical significance was determined using the Holm-Sidak method, with alpha = 0.05. Each row was analyzed individually, without assuming a consistent SD

alter gene expression within individual cell line pairs (e.g., MCF10A-sh:p53 vs. MCF10A-sh:GFP), or elicit a common transcriptional response across the 3 pre-malignant lines (i.e., all 3 sh:p53 samples vs. all 3 sh:GFP controls; not shown).

Conversely, in the context of RMFs, *TP53* knockdown was associated with more striking transcriptional changes. To characterize the stromal reaction of pre-invasive, p53-deficient BBCs, we performed a 2-class unpaired SAM comparing MCF10A-sh:p53, MCF10AT1-sh:p53, and MCF10DCIS-sh:p53 co-cultures to the corresponding *TP53*-knockdown epithelial mono-cultures. This analysis revealed that, in the setting of p53 deficiency, 38 genes

were significantly upregulated in response to stroma (false discovery rate [FDR] = 4.37%; Fig. 2a, Suppl. Table 1); the expression level of each of these genes was highly correlated between biological replicates (r > 0.80 for each sample pair; Suppl. Figure 3b). Importantly, none of these genes were significantly different between p53-sufficient co-cultures and the corresponding epithelial-monocultures (FDR = 0%), demonstrating that expression of the progression signature is dependent upon epithelial p53 status. IPA revealed that this gene set, herein referred to as the "progression signature", was enriched for pathways such as hepatic fibrosis/hepatic stellate cell activation, interleukin-17A

Fig. 2 Expression of an MCF10 series-based progression gene signature persists in the setting of invasive basal-like breast cancer. **a**) Heat map depicting genes that are significantly differentially expressed in p53-deficient co-cultures vs. epithelial mono-cultures (the "progression signature"). Fold change is relative to median expression. **b**) Invasive breast cancer cell-fibroblast (RMF) co-cultures from the Camp et al. dataset (ref. 20) were scored for the progression signature. Data from two types of co-culture models were analyzed, including cultures in which both RMFs and cancer cells were grown in physical contact in the same culture well ("direct" co-cultures, left), and cultures in which both cell types were physically separated

but in contact via soluble mediators secreted into the culture medium ("indirect" co-cultures, right). ***$p = 0.0009$. Statistical significance was determined using the Holm-Sidak method, with alpha = 0.05. Each row was analyzed individually, without assuming a consistent SD. Number of t tests: 4. **c**) Expression of the progression signature in human breast tumor specimens from The Cancer Genome Atlas (TCGA; n = 1054). ****$p < 0.0001$ by one-way ANOVA with Tukey's multiple comparisons test. **d**) Expression of the progression signature in human breast tumor specimens from the METABRIC dataset (n = 1689). ***$p = 0.0001$; ****$p < 0.0001$ by one-way ANOVA with Tukey's multiple comparisons test

(IL-17A) signaling in fibroblasts, role of IL-17F in allergic inflammatory airway diseases, and regulation of the epithelial-mesenchymal transition pathway (Benjamini-Hochberg-corrected p values of 2.71×10^{-9}, 0.0176, 0.0247, and 0.0293, respectively). To confirm that RMFs were not a major contributor to progression signature gene expression, we performed a 2-class SAM comparing p53-deficient co-cultures to RMF mono-cultures; significant differential expression of 7093 genes was observed (FDR = 4.78%; Suppl. Figure 3c; Suppl. Table 2). As expected, fibroblast

marker genes (*S100A4*, *ACTA2*); collagen and fibronectin genes (*COL1A1*, *COL1A2*, *COL5A2*, *COL6A2*, *COL8A1*, *COL10A1*, *COL13A1*, *COL15A1*, *COL18A1*, and *FN1*); and genes encoding extracellular matrix synthesis and modifying proteins (*LOXL1*, *LOXL3*, *LOXL4*, *PCOLCE*, *PCOLCE2*, *PLOD2*, and *SERPINH1*) were significantly upregulated in RMFs relative to p53-deficient co-cultures. We also observed that 35/38 progression signature genes (92.1%) were significantly differentially expressed between p53-deficient co-cultures and RMFs; only *LCE2A*, *IL6*, and

RHCG were unchanged between these two groups. Taken together, these results confirm that the progression signature reflects the contribution of both stromal and epithelial cells, as well as heterotypic interactions between them.

Evaluation of the Progression Signature in Invasive BBC Cell Lines and Human Tumor Tissue

Previous human tissue studies have demonstrated that the majority of transcriptional changes associated with breast cancer progression – in both the epithelial and stromal tissue compartments – are present in pre-invasive tissue [6, 7]. Therefore, having identified a gene signature associated with exposure of pre-invasive, p53-deficient BBC cell lines to fibroblasts, we hypothesized that these transcriptional patterns would be associated with tumor subtype in the setting of invasive breast cancer. Using the cell-based dataset reported by Camp and colleagues [20], we first tested whether the progression signature was upregulated in co-culture models of invasive basal-like vs. luminal cancers. The Camp et al. study [20] employed 2 distinct co-culture models, including "direct" co-cultures, wherein both cell types (cancer cells and RMFs) were grown in direct contact in the same culture well, and "indirect" co-cultures, wherein the two cell types were separated by a porous barrier that prevented physical contact but still

enabled cell–cell communication via soluble signaling mediators. The breast cancer cell lines included in this analysis, as well as the *TP53* statuses thereof, are presented in Table 1. Importantly, although SUM102-PT BBC cells express wild-type *TP53*, we included this cell line in our analysis because it exhibits other deleterious p53 pathway defects including p14*ARF* deletion and *CHEK2* loss of function [32]. In addition, due to the relatively low number of luminal breast cancer co-culture models in this dataset, we classified HER2-amplified SKBR3 cells as "luminal" in this analysis because 1) this cell line was also classified as "luminal" by Neve and colleagues [33], and 2) previous cell-based research suggests that HER2-enriched and luminal breast cancers may share similar microenvironmental characteristics [20]. Among the "direct" co-cultures, the progression signature tended to be more highly expressed in basal-like relative to luminal co-cultures under all conditions examined, but these relationships were not statistically significant (Fig. 2b). The magnitude of progression signature expression also increased with increasing ratio of RMFs to epithelial cells (Fig. 2b). Moreover, the progression signature was significantly upregulated in "indirect" co-culture models of basal-like vs. luminal breast cancers (Fig. 2b).

In human bulk tumor tissue, we also observed upregulation of the in vitro progression signature

Table 1 Co-culture models of invasive breast cancer from the Camp et al. dataset (ref. 20) scored for the progression signature

Cell line	PAM50 subtype[a]	Co-culture model(s)	*TP53* status; protein change	Reference(s)
HCC1937	Basal-like	Direct	LOH; mutant (nonsense; R306*)	(38,39)
MDA-MB-231	Basal-like	Direct	Mutant (missense; R280K)	(39)
MDA-MB-468	Basal-like	Direct	Mutant (missense; R273H)	(39)
SUM102-PT	Basal-like	Direct, indirect	Wild-type[b]	(20,39)
SUM149-PT	Basal-like	Direct, indirect	LOH; mutant (missense; M237I)	(39)
SUM159-PT	Basal-like	Direct	LOH; mutant (missense; S158insS)	(39)
MCF7	Luminal	Direct, indirect	Wild-type	(11,39)
SKBR3	HER2[c]	Direct	Mutant (missense; R175H)	(11,39)
T47D	Luminal	Direct, indirect	Mutant (missense; L194F)	(39)
ZR-75–1	Luminal	Direct	Wild-type	(39)

[a]The PAM50 subtype reported for each cell line was determined by Camp and colleagues (20)

[b]*TP53*-wild-type SUM102 cells were included in this analysis because they exhibit other deleterious defects in p53 pathway function including *CHEK2* loss of function and p14*ARF* deletion (32)

[c]Although SKBR3 cells were reported to be a model of HER2-enriched breast cancer in (20), we classified this cell line as "luminal" in the present analysis because 1) this cell line was also classified as "luminal" in (33); 2) HER2-enriched and luminal breast cancers may share similar microenvironmental characteristics (20); and 3) a limited number of luminal co-culture models (relative to basal-like co-culture models) was represented in the Camp et al. dataset (20)

among BBCs. In both the TCGA (n = 1054; [12]) and METABRIC (n = 1689; [27]) breast cancer datasets, the progression signature was significantly enriched in basal-like relative to luminal A and/or luminal B cancers (Fig. 2c-d). Interestingly, the signature was also more highly expressed in HER2-enriched relative to luminal B tumors (Fig. 2c-d). Collectively, these data demonstrate that the stromal responses of pre-malignant, p53-deficient BBCs are active at later stages of progression, in invasive basal-like disease.

Discussion

Studies of heterotypic interactions during carcinogenesis are critical for understanding how pre-invasive cells overcome microenvironmental barriers to malignancy. Given the high prevalence of deleterious (nonsense and frameshift) *TP53* mutations in basal-like breast tumors [12], it is also important to evaluate effects of p53 deficiency on BBC carcinogenesis, particularly in the context of stromal-epithelial interactions. Herein, we used a quantitative, OCT-based morphology assay and genome-wide expression analyses to identify cancer cell-intrinsic and microenvironmental factors associated with BBC carcinogenesis. Phenotypic responses of pre-invasive BBCs to fibroblast co-culture were dependent upon genetic context, with *TP53*-knockdown acini exhibiting more dramatic stoma-induced increases in asphericity/cell invasive potential compared to p53-sufficient controls. We also identified a transcriptional signature upregulated in pre-malignant, *TP53*-knockdown co-cultures, providing insight into stromal-epithelial communication patterns that may induce or sustain adaptive epithelial phenotypes during early stages of p53-deficient BBC initiation.

The 38-gene progression signature identified in this study, which is associated with increased acinus asphericity, reflects transcriptional responses of p53-deficient benign (MCF10A), atypical hyperplastic (MCF10AT1), and DCIS (MCF10DCIS) acini to fibroblasts. That this signature is also upregulated in basal-like tumor tissue and cell-based models of invasive BBC corroborates previous data suggesting that stromal-epithelial communication patterns established during early stages of BBC carcinogenesis may also play important roles in the setting of malignancy [6, 7]. Interestingly, the progression signature was enriched for genes associated with IL-17 and hepatic fibrosis signaling, including *COL1A2*, *COL10A1*, *IL6*, *IL11*, *LY96*, *MMP1*, *MMP2*, *MYL9*, *PDGFRA*, and *PDGFRB*. IL-17 is a pro-inflammatory, pro-fibrotic cytokine, expression of which in breast cancers is associated with reduced disease-free survival and poor prognostic tumor features such as triple-negative subtype, estrogen receptor (ER) and/

or progesterone receptor (PR) negativity, and high grade [34–44]. In addition, treatment of invasive BBC cell lines with IL-17 promotes cell proliferation, migration, invasion, and chemoresistance [35, 39, 40], whereas in vivo IL-17 blockade reduces ER-negative and triple-negative breast tumor burden and metastasis by suppressing pro-tumorigenic immune responses [36, 37, 41]. Furthermore, inverse associations between serum IL-17 levels and tumor p53 expression have been reported in patients with colorectal cancer [42], whereas IL-17A-mediated suppression of p53 has recently been shown to promote therapeutic resistance in B cell lymphoma [43, 44]. Therefore, the potential implications of molecular crosstalk between IL-17 and p53 in the setting of pre-malignant and invasive BBC warrant further investigation.

In contrast to co-cultures, wherein all three p53-deficient breast cell lines became significantly more aspherical in the presence of RMFs, *TP53* knockdown exerted minimal morphogenetic effects in mono-culture, significantly increasing the asphericity of benign MCF10A acini only. In addition, p53 deficiency alone was insufficient to significantly influence gene expression in any of the MCF10 cell lines studied. This result is in line with the well-established role of p53 as a regulator of cell stress responses, and corroborates our previous work demonstrating only modest transcriptional responses to p53 depletion in malignant breast cancer cells [11]. For example, in this study [11], the gene expression profiles of *TP53*-wild-type MCF7 cells were unchanged following *TP53* knockdown. However, nearly 600 genes were differentially expressed in association with MCF7 p53 status following treatment with the DNA-intercalating agent, doxorubicin [11]. Accordingly, considering the role of p53 as a master regulator of genome stability, together with the relatively small mutational burden of pre-invasive breast cancer cells, a broader range of p53-dependent transcriptional alterations would be expected in MCF10 series acini exposed to cellular stressors such as DNA damage, nutrient deprivation, or hypoxia.

Our data should be interpreted in view of the characteristics of our model system. For instance, compared to a previous study of MCF10 series-fibroblast interactions in 2D cultures [9], the present study identified far fewer transcriptional alterations induced by the presence of stroma. The relatively limited gene expression changes identified in 3D cultures may have arisen due to the inhibitory effect of basement membrane proteins on cell signaling [45, 46], as a result of biomechanical considerations pertaining to cell growth within a semi-solid matrix vs. on plastic, differences in physical cell–cell contact, and/or variations in the diffusibility of soluble signaling mediators. We also note that the percentage of RMFs was substantially lower in our 3D cultures, as the fibroblasts proliferated much

more slowly than the epithelium. In contrast, in 2D cultures, fibroblasts and MCF10 series cells exhibit similar population doubling times. Nonetheless, in our model, stroma-induced gene expression changes accumulated over a two-week period, including during early days of 3D culture when the proportions of each cell type were roughly equivalent. The transcriptional patterns at later time points, such as those analyzed here, are best interpreted as reflective of long-term, steady-state responses to co-culture and/or morphologic changes induced therein.

In conclusion, our study demonstrated that stromal-epithelial interactions during early stages of BBC carcinogenesis depend upon epithelial p53 status, and provided novel insights into patterns of molecular crosstalk that may induce or sustain adaptive epithelial phenotypes during the development of this tumor subtype. Although 3D cultures contain a limited number of cell types and thus do not reflect the full dynamic complexity of living tissues, our data and that of others [8, 9, 23, 47–49] strongly suggest that these models can successfully recapitulate known aspects of breast tissue biology. Future research integrating transcriptional analyses and quantitative phenotypic assays may lead to the identification of additional targetable microenvironment interactions in BBC.

Authors' Contributions Conceptualization: Ashley M. Fuller, Melissa A. Troester; Methodology: Ashley M. Fuller, Lin Yang, Jason R. Pirone, Amy L. Oldenburg, Alina M. Hamilton; Formal analysis and investigation: Ashley M. Fuller; Writing—original draft preparation: Ashley M. Fuller; Writing—review and editing: Ashley M. Fuller, Lin Yang, Alina M. Hamilton, Jason R. Pirone, Amy L. Oldenburg, Melissa A. Troester; Funding acquisition: Ashley M. Fuller, Amy L. Oldenburg, Melissa A. Troester; Resources: Amy L. Oldenburg, Melissa A. Troester; Supervision: Melissa A. Troester.

Availability of Data and Materials The datasets generated during the current study are available in the NCBI Gene Expression Omnibus (GSE162553). Other materials generated during this study are available from the corresponding author upon reasonable request.

Code Availability The code utilized in this study is available from the corresponding author upon reasonable request.

Compliance with Ethical Standards

Conflicts of Interest The authors declare no potential conflicts of interest.

Ethics Approval This article does not contain any studies with human participants or animals performed by any of the authors.

Consent to Participate This article does not contain any studies with human participants performed by any of the authors.

Consent for Publication This manuscript has been approved by all co-authors.

References

1. Bombonati A, Sgroi DC. The molecular pathology of breast cancer progression. J Pathol. 2011;223:307–17. https://doi.org/10.1002/path.2808.

2. Sgroi DC. Preinvasive breast cancer. Annu Rev Pathol. 2010;5:193–221. https://doi.org/10.1146/annurev.pathol.4.110807.092306.

3. Allinen M, Beroukhim R, Cai L, Brennan C, Lahti-Domenici J, Huang H, Porter D, Hu M, Chin L, Richardson A, Schnitt S, Sellers WR, Polyak K. Molecular characterization of the tumor microenvironment in breast cancer. Cancer Cell. 2004;6:17–32. https://doi.org/10.1016/j.ccr.2004.06.010.

4. Cichon MA, Degnim AC, Visscher DW, Radisky DC. Microenvironmental influences that drive progression from benign breast disease to invasive breast cancer. J Mammary Gland Biol Neoplasia. 2010;15:389–97. https://doi.org/10.1007/s10911-010-9195-8.

5. Hu M, Yao J, Carroll DK, Weremowicz S, Chen H, Carrasco D, Richardson A, Violette S, Nikolskaya T, Nikolsky Y, Bauerlein EL, Hahn WC, Gelman RS, Allred C, Bissell MJ, Schnitt S, Polyak K. Regulation of in situ to invasive breast carcinoma transition. Cancer Cell. 2008;13:394–406. https://doi.org/10.1016/j.ccr.2008.03.007.

6. Ma XJ, Salunga R, Tuggle JT, Gaudet J, Enright E, McQuary P, Payette T, Pistone M, Stecker K, Zhang BM, Zhou YX, Varnholt H, Smith B, Gadd M, Chatfield E, Kessler J, Baer TM, Erlander MG, Sgroi DC. Gene expression profiles of human breast cancer progression. Proc Natl Acad Sci U S A. 2003;100:5974–9. https://doi.org/10.1073/pnas.0931261100.

7. Ma XJ, Dahiya S, Richardson E, Erlander M, Sgroi DC. Gene expression profiling of the tumor microenvironment during breast cancer progression. Breast Cancer Res. 2009;11:R7. https://doi.org/10.1186/bcr2222.

8. Chhetri RK, Phillips ZF, Troester MA, Oldenburg AL. Longitudinal study of mammary epithelial and fibroblast co-cultures using optical coherence tomography reveals morphological hallmarks of pre-malignancy. PLoS ONE. 2012;7:e49148. https://doi.org/10.1371/journal.pone.0049148.

9. Casbas-Hernandez P, D'Arcy M, Roman-Perez E, Brauer HA, McNaughton K, Miller SM, Chhetri RK, Oldenburg AL, Fleming JM, Amos KD, Makowski L, Troester MA. Role of HGF in epithelial-stromal cell interactions during progression from benign breast disease to ductal carcinoma in situ. Breast Cancer Res. 2013;15:R82. https://doi.org/10.1186/bcr3476.

10. Carey LA, Perou CM, Livasy CA, Dressler LG, Cowan D, Conway K, Karaca G, Troester MA, Tse CK, Edmiston S, Deming SL, Geradts J, Cheang MC, Nielsen TO, Moorman PG, Earp HS, Millikan RC. Race, breast cancer subtypes, and survival

in the Carolina Breast Cancer Study. JAMA. 2006;295:2492–502. https://doi.org/10.1001/jama.295.21.2492.

11. Troester MA, Herschkowitz JI, Oh DS, He X, Hoadley KA, Barbier CS, Perou CM. Gene expression patterns associated with p53 status in breast cancer. BMC Cancer. 2006;6:276. https://doi.org/10.1186/1471-2407-6-276.

12. Cancer Genome Atlas N. Comprehensive molecular portraits of human breast tumours. Nature. 2012;490:61–70. https://doi.org/10.1038/nature11412.

13. Basolo F, Elliott J, Tait L, Chen XQ, Maloney T, Russo IH, Pauley R, Momiki S, Caamano J, Klein-Szanto AJ, et al. Transformation of human breast epithelial cells by c-Ha-ras oncogene. Mol Carcinog. 1991;4:25–35. https://doi.org/10.1002/mc.2940040106.

14. Chavez KJ, Garimella SV, Lipkowitz S. Triple negative breast cancer cell lines: one tool in the search for better treatment of triple negative breast cancer. Breast Dis. 2010;32:35–48. https://doi.org/10.3233/BD-2010-0307.

15. Sarrio D, Rodriguez-Pinilla SM, Hardisson D, Cano A, Moreno-Bueno G, Palacios J. Epithelial-mesenchymal transition in breast cancer relates to the basal-like phenotype. Cancer Res. 2008;68:989–97. https://doi.org/10.1158/0008-5472.CAN-07-2017.

16. Miller FR, Soule HD, Tait L, Pauley RJ, Wolman SR, Dawson PJ, Heppner GH. Xenograft model of progressive human proliferative breast disease. J Natl Cancer Inst. 1993;85:1725–32. https://doi.org/10.1093/jnci/85.21.1725.

17. Dawson PJ, Wolman SR, Tait L, Heppner GH, Miller FR. MCF10AT: a model for the evolution of cancer from proliferative breast disease. Am J Pathol. 1996;148:313–9.

18. Miller FR, Santner SJ, Tait L, Dawson PJ. MCF10DCIS.com xenograft model of human comedo ductal carcinoma in situ. J Natl Cancer Inst. 2000;92:1185–6. https://doi.org/10.1093/jnci/92.14.1185a.

19. Hu X, Stern HM, Ge L, O'Brien C, Haydu L, Honchell CD, Haverty PM, Peters BA, Wu TD, Amler LC, Chant J, Stokoe D, Lackner MR, Cavet G. Genetic alterations and oncogenic pathways associated with breast cancer subtypes. Mol Cancer Res. 2009;7:511–22. https://doi.org/10.1158/1541-7786.MCR-08-0107.

20. Camp JT, Elloumi F, Roman-Perez E, Rein J, Stewart DA, Harrell JC, Perou CM, Troester MA. Interactions with fibroblasts are distinct in Basal-like and luminal breast cancers. Mol Cancer Res. 2011;9:3–13. https://doi.org/10.1158/1541-7786.MCR-10-0372.

21. Masutomi K, Yu EY, Khurts S, Ben-Porath I, Currier JL, Metz GB, Brooks MW, Kaneko S, Murakami S, DeCaprio JA, Weinberg RA, Stewart SA, Hahn WC. Telomerase maintains telomere structure in normal human cells. Cell. 2003;114:241–53.

22. Johnson KR, Leight JL, Weaver VM. Demystifying the effects of a three-dimensional microenvironment in tissue morphogenesis. Methods Cell Biol. 2007;83:547–83. https://doi.org/10.1016/S0091-679X(07)83023-8.

23. Yu X, Fuller AM, Blackmon R, Troester MA, Oldenburg AL. Quantification of the Effect of Toxicants on the Intracellular Kinetic Energy and Cross-Sectional Area of Mammary Epithelial Organoids by OCT Fluctuation Spectroscopy. Toxicol Sci. 2018;162:234–40. https://doi.org/10.1093/toxsci/kfx245.

24. Krawitz BD, Mo S, Geyman LS, Agemy SA, Scripsema NK, Garcia PM, Chui TYP, Rosen RB. Acircularity index and axis ratio of the foveal avascular zone in diabetic eyes and healthy controls measured by optical coherence tomography angiography. Vision Res. 2017;139:177–86. https://doi.org/10.1016/j.visres.2016.09.019.

25. Buess M, Nuyten DS, Hastie T, Nielsen T, Pesich R, Brown PO. Characterization of heterotypic interaction effects in vitro to deconvolute global gene expression profiles in cancer. Genome Biol. 2007;8:R191. https://doi.org/10.1186/gb-2007-8-9-r191.

26. Creighton CJ, Casa A, Lazard Z, Huang S, Tsimelzon A, Hilsenbeck SG, Osborne CK, Lee AV. Insulin-like growth factor-I activates gene transcription programs strongly associated with poor breast cancer prognosis. J Clin Oncol. 2008;26:4078–85. https://doi.org/10.1200/JCO.2007.13.4429.

27. Curtis C, Shah SP, Chin SF, Turashvili G, Rueda OM, Dunning MJ, Speed D, Lynch AG, Samarajiwa S, Yuan Y, Graf S, Ha G, Haffari G, Bashashati A, Russell R, McKinney S, Group M, Langerod A, Green A, Provenzano E, Wishart G, Pinder S, Watson P, Markowetz F, Murphy L, Ellis I, Purushotham A, Borresen-Dale AL, Brenton JD, Tavare S, Caldas C, Aparicio S. The genomic and transcriptomic architecture of 2,000 breast tumours reveals novel subgroups. Nature. 2012;486:346–52. https://doi.org/10.1038/nature10983.

28. Freed-Pastor WA, Mizuno H, Zhao X, Langerod A, Moon SH, Rodriguez-Barrueco R, Barsotti A, Chicas A, Li W, Polotskaia A, Bissell MJ, Osborne TF, Tian B, Lowe SW, Silva JM, Borresen-Dale AL, Levine AJ, Bargonetti J, Prives C. Mutant p53 disrupts mammary tissue architecture via the mevalonate pathway. Cell. 2012;148:244–58. https://doi.org/10.1016/j.cell.2011.12.017.

29. Weiss MB, Vitolo MI, Mohseni M, Rosen DM, Denmeade SR, Park BH, Weber DJ, Bachman KE. Deletion of p53 in human mammary epithelial cells causes chromosomal instability and altered therapeutic response. Oncogene. 2010;29:4715–24. https://doi.org/10.1038/onc.2010.220.

30. Zhang Y, Yan W, Chen X. Mutant p53 disrupts MCF-10A cell polarity in three-dimensional culture via epithelial-to-mesenchymal transitions. J Biol Chem. 2011;286:16218–28. https://doi.org/10.1074/jbc.M110.214585.

31. EJ Pereira JS Burns CY Lee T Marohl D Calderon L Wang KA Atkins CC Wang KA Janes 2020 Sporadic activation of an oxidative stress-dependent NRF2-p53 signaling network in breast epithelial spheroids and premalignancies Sci Signal 13 https://doi.org/10.1126/scisignal.aba4200

32. Barnabas N, Cohen D. Phenotypic and Molecular Characterization of MCF10DCIS and SUM Breast Cancer Cell Lines. Int J Breast Cancer. 2013;2013:872743. https://doi.org/10.1155/2013/872743.

33. Neve RM, Chin K, Fridlyand J, Yeh J, Baehner FL, Fevr T, Clark L, Bayani N, Coppe JP, Tong F, Speed T, Spellman PT, DeVries S, Lapuk A, Wang NJ, Kuo WL, Stilwell JL, Pinkel D, Albertson DG, Waldman FM, McCormick F, Dickson RB, Johnson MD, Lippman M, Ethier S, Gazdar A, Gray JW. A collection of breast cancer cell lines for the study of functionally distinct cancer subtypes. Cancer Cell. 2006;10:515–27. https://doi.org/10.1016/j.ccr.2006.10.008.

34. Chen WC, Lai YH, Chen HY, Guo HR, Su IJ, Chen HH. Interleukin-17-producing cell infiltration in the breast cancer tumour microenvironment is a poor prognostic factor. Histopathology. 2013;63:225–33. https://doi.org/10.1111/his.12156.

35. Cochaud S, Giustiniani J, Thomas C, Laprevotte E, Garbar C, Savoye AM, Cure H, Mascaux C, Alberici G, Bonnefoy N, Eliaou JF, Bensussan A, Bastid J. IL-17A is produced by breast cancer TILs and promotes chemoresistance and proliferation through ERK1/2. Sci Rep. 2013;3:3456. https://doi.org/10.1038/srep03456.

36. Benevides L, da Fonseca DM, Donate PB, Tiezzi DG, De Carvalho DD, de Andrade JM, Martins GA, Silva JS. IL17 Promotes Mammary Tumor Progression by Changing the Behavior of Tumor Cells and Eliciting Tumorigenic Neutrophils Recruitment. Cancer Res. 2015;75:3788–99. https://doi.org/10.1158/0008-5472.CAN-15-0054.

37. Ma YF, Chen C, Li D, Liu M, Lv ZW, Ji Y, Xu J. Targeting of interleukin (IL)-17A inhibits PDL1 expression in tumor cells and induces anticancer immunity in an estrogen receptor-negative murine model of breast cancer. Oncotarget. 2017;8:7614–24. https://doi.org/10.18632/oncotarget.13819.

38. Benevides L, Cardoso CR, Tiezzi DG, Marana HR, Andrade JM, Silva JS. Enrichment of regulatory T cells in invasive breast

tumor correlates with the upregulation of IL-17A expression and invasiveness of the tumor. Eur J Immunol. 2013;43:1518–28. https://doi.org/10.1002/eji.201242951.

39. Zhu X, Mulcahy LA, Mohammed RA, Lee AH, Franks HA, Kilpatrick L, Yilmazer A, Paish EC, Ellis IO, Patel PM, Jackson AM. IL-17 expression by breast-cancer-associated macrophages: IL-17 promotes invasiveness of breast cancer cell lines. Breast Cancer Res. 2008;10:R95. https://doi.org/10.1186/bcr2195.

40. Changchun K, Pengchao H, Ke S, Ying W, Lei W. Interleukin-17 augments tumor necrosis factor alpha-mediated increase of hypoxia-inducible factor-1alpha and inhibits vasodilator-stimulated phosphoprotein expression to reduce the adhesion of breast cancer cells. Oncol Lett. 2017;13:3253–60. https://doi.org/10.3892/ol.2017.5825.

41. Coffelt SB, Kersten K, Doornebal CW, Weiden J, Vrijland K, Hau CS, Verstegen NJM, Ciampricotti M, Hawinkels L, Jonkers J, de Visser KE. IL-17-producing gammadelta T cells and neutrophils conspire to promote breast cancer metastasis. Nature. 2015;522:345–8. https://doi.org/10.1038/nature14282.

42. Radosavljevic G, Ljujic B, Jovanovic I, Srzentic Z, Pavlovic S, Zdravkovic N, Milovanovic M, Bankovic D, Knezevic M, Acimovic LJ, Arsenijevic N. Interleukin-17 may be a valuable serum tumor marker in patients with colorectal carcinoma. Neoplasma. 2010;57:135–44.

43. Li Q, Xu X, Zhong W, Du Q, Yu B, Xiong H. IL-17 induces radiation resistance of B lymphoma cells by suppressing p53 expression and thereby inhibiting irradiation-triggered apoptosis. Cell Mol Immunol. 2015;12:366–72. https://doi.org/10.1038/cmi.2014.122.

44. Zhong W, Xu X, Zhu Z, Yang L, Du H, Xia Z, Yuan Z, Xiong H, Du Q, Wei Y, Li Q. Increased interleukin-17A levels promote rituximab resistance by suppressing p53 expression and predict an unfavorable prognosis in patients with diffuse large B cell lymphoma. Int J Oncol. 2018. https://doi.org/10.3892/ijo.2018.4299.

45. Petersen OW, Ronnov-Jessen L, Howlett AR, Bissell MJ. Interaction with basement membrane serves to rapidly distinguish growth and differentiation pattern of normal and malignant human breast epithelial cells. Proc Natl Acad Sci U S A. 1992;89:9064–8.

46. Weaver VM, Petersen OW, Wang F, Larabell CA, Briand P, Damsky C, Bissell MJ. Reversion of the malignant phenotype of human breast cells in three-dimensional culture and in vivo by integrin blocking antibodies. J Cell Biol. 1997;137:231–45.

47. Lee GY, Kenny PA, Lee EH, Bissell MJ. Three-dimensional culture models of normal and malignant breast epithelial cells. Nat Methods. 2007;4:359–65. https://doi.org/10.1038/nmeth1015.

48. Sadlonova A, Bowe DB, Novak Z, Mukherjee S, Duncan VE, Page GP, Frost AR. Identification of molecular distinctions between normal breast-associated fibroblasts and breast cancer-associated fibroblasts. Cancer Microenviron. 2009;2:9–21. https://doi.org/10.1007/s12307-008-0017-0.

49. Sadlonova A, Novak Z, Johnson MR, Bowe DB, Gault SR, Page GP, Thottassery JV, Welch DR, Frost AR. Breast fibroblasts modulate epithelial cell proliferation in three-dimensional in vitro co-culture. Breast Cancer Res. 2005;7:R46-59. https://doi.org/10.1186/bcr949.